Dynamics of two vibro-impact nonlinear energy sinks in parallel under periodic and transient excitations

Tao Li, Etienne Gourc, Sébastien Seguy, Alain Berlioz

▶ To cite this version:

HAL Id: hal-01820032
https://hal.insa-toulouse.fr/hal-01820032

Submitted on 3 Dec 2018

Dynamics of two vibro-impact nonlinear energy sinks in parallel under periodic and transient excitations

T. Li[a,], E. Gourc[b], S. Seguy[a], A. Berlioz[a]

[a]*Université de Toulouse, Institut Clément Ader (ICA), CNRS-INSA-ISAE-Mines Albi-UPS,Toulouse, France*
[b]*Space Structures and Systems Laboratory, Department of Aerospace and Mechanical Engineering, University of Liege, 1 Chemin des Chevreuils (B52/3), B-4000 Liege, Belgium*

Abstract

A linear oscillator (LO) coupled with two vibro-impact (VI) nonlinear energy sinks (NES) in parallel is studied under periodic and transient excitations, respectively. The objective is to study response regimes and to compare their efficiency of vibration control. Through the analytical study with multiple scales method, two slow invariant manifolds (SIM) are obtained for two VI NES, and different SIM that result from different clearances analytically supports the principle of separate activation. In addition, fixed points are calculated and their positions are applied to judge response regimes. Transient responses and modulated responses can be further explained. By this way, all analysis is around the most efficient response regime. Then, numerical results demonstrate two typical responses and validate the effectiveness of analytical prediction. Finally, basic response regimes are experimentally observed and analyzed, and they can well explain the complicated variation of responses and their corresponding efficiency, not only for periodic excitations with a fixed frequency or a range of frequency, but also for transient excitation. Generally, vibration control is more effective when VI NES is activated with two impacts per cycle, whatever the types of excitation and the

25 combinations of clearances. This observation is also well reflected by the separate

26 activation of two VI NES with two different clearances, but at different levels of

27 displacement amplitude of LO.

28 *Keywords:* Vibro-impact, Targeted energy transfer, Nonlinear energy sink,

29 Impact damper

30 1. Introduction

31   The excessive vibration energy of a targeted system can be dissipated by using

32 an auxiliary device, which absorbs and dissipates such undesired energy by pro-

33 ducing a force opposing it, either continuously such as in the case of nonlinear en-

34 ergy sink (NES) with continuous nonlinearity [1, 2, 3, 4, 5] or segmentally by NES

35 with piece-wise nonlinearity [6] or intermittently and instantly by impact damper

36 [7]. Due to its simplicity of construction, fast response at the initial stage of per-

37 turbation and effectiveness at a broadband frequency, impact damper has been

38 studied several decades ago [8, 9], no matter the case with only one impact pair

39 [10, 11, 12, 13, 14] or multi-units with several impact-pairs [15, 16, 17, 18, 19, 20].

40   Recently, impact damper is studied further and more clear under the context

41 of targeted energy transfer (TET) [21, 22] and termed as vibro-impact (VI) NES

42 [23, 24, 25]. Its mechanism of TET is revealed by studying its Hamiltonian system

43 [26], and it is observed that some special orbits are responsible for the irreversible

44 transfer of energy from a main system to an attached VI NES. Through directly

45 studying the system with damping, a slow invariant manifold (SIM), which is

46 firstly used for the analysis of a NES with cubic nonlinearity [27, 28], can be

47 obtained by multiple scales method and be applied to analyze response regimes

48 [29, 30, 31, 32, 33]. As a result, transient responses and unsteady responses such

2

49 as chaotic strongly modulated response (SMR) can be well explained for the first

50 time [31, 34]. Dynamics, such as response regimes and bifurcations, is compre-

51 hensively re-analyzed around SIM [35], more specifically, around the regime with

52 two impacts per cycle. In [36], the efficiency of different response regimes around

53 SIM is compared, and the response regime with two impact per cycle and around

54 the entrance of SMR is found to be optimal. Based on this efficiency compari-

55 son of response regimes, a common optimization design criterion of VI NES is

56 proposed for different excitation types, and the central idea is to make the most

57 efficient response regime with two impacts per cycle exist or last as long as pos-

58 sible. Therefore, it is natural to expect the following design criterion for multi VI

59 NES: to make each VI NES activated with this optimal response regime.

60   About its application, any analytical study of nonlinear systems coupled with

61 NES will be difficult, no matter this nonlinear system is a turning system [37]

62 or a helicopter system [38], or even a simple rod [39]. For VI NES, a solution

63 is to found its activation condition without considering the specific type of a tar-

64 geted system. It is found that the activation of a VI NES is limited to a range of

65 displacement amplitude of a linear system [36]. From the viewpoint of energy,

66 it means that its effectiveness is not only limited by a minimal value (activation

67 threshold) but also a maximal value. Therefore, it is natural to increase the range

68 of effectiveness of vibration control by designing different VI NES with different

69 activation ranges for both linear and nonlinear systems. In this way, the efficiency

70 and robustness of TET can be improved, even at small energy levels.

71   About multi NES, there already exist extensive studies [40, 41, 42, 43], and

72 normally frequency components are used as indices to judge the possible tran-

73 sient or sustained resonance captures, and to identify different levels of activation.

3

74 However, this kind of index will not be used here for VI NES, since the impact

75 number per cycle is a more direct measure. For example, the response regime with

76 two impacts per cycle can be easily distinguished from numerical or experimen-

77 tal viewpoints, and actually it corresponds to 1:1 resonance. Although frequency

78 components can be calculated by wavelet transform, it will not make the analysis

79 easier and will not be used here.

80 In addition to the viewpoint of TET, the analytical study of systems coupled

81 with multi VI NES also deserves further investigation fortwo reasons. Firstly, the

82 research of multi VI NES is closely related to particle dampers [44]. Secondly,

83 complicated response regimes such as intermittent beating responses [18, 19] need

84 further analytical explanations rather than only analytical treatments of steady

85 periodic regimes [16, 20].

86 Therefore, the objective of this paper is to generalize the optimization design

87 criterion for one VI NES [36] to multiple VI NES. The focus is still around re-

88 sponse regimes, efficiency and the relation between them. The impact number per

89 cycle is used to characterize response regimes and corresponding TET.

90 The paper is organized as follows: a linear oscillator (LO) coupled with two VI

91 NES in parallel under periodic excitation is analytically developed in Section 2.

92 Then, numerical validations are demonstrated. In Section 4, experimental results

93 under periodic and transient excitations are demonstrated for different conditions.

94 Finally, a conclusion is addressed.

95 **2. Analytical development**

96 The considered system is presented in Fig. 1. Two VI NES in parallel are

97 attached to a LO. The equation of motion between impacts is expressed as follows:
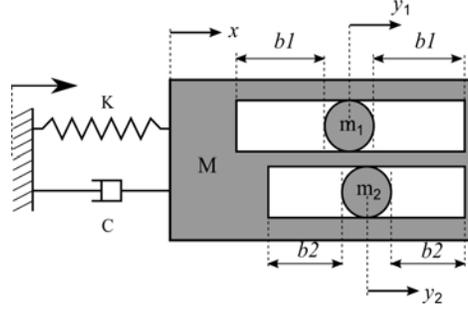
4

Fig. 1. Schema of a LO with two VI NES coupled in parallel.

$$M\frac{d^2x}{dt^2} + C\frac{dx}{dt} + Kx = F\sin\Omega t$$
$$m_1\frac{d^2y_1}{dt^2} = 0, \quad \forall|x-y_1| < b1 \tag{1}$$
$$m_2\frac{d^2y_2}{dt^2} = 0, \quad \forall|x-y_2| < b2$$

⁹⁸ The motion relation between states before and after impacts can be obtained
⁹⁹ under the condition of simplified impact theory and conservation of momentum
¹⁰⁰ and it can be written as:

$$\forall|x-y_1| = b1 \quad \text{or} \quad |x-y_2| = b2$$
$$x_+ = x_-, \quad y_{1+} = y_{1-}, \quad y_{2+} = y_{2-}$$
$$M\frac{dx_+}{dt} + m_1\frac{dy_{1+}}{dt} + m_2\frac{dy_{2+}}{dt} = M\frac{dx_-}{dt} + m_1\frac{dy_{1-}}{dt} + m_2\frac{dy_{2-}}{dt}$$
$$\text{if } |x-y_1| = b1 \tag{2}$$
$$\frac{dx_+}{dt} - \frac{dy_{1+}}{dt} = -R\left(\frac{dx_-}{dt} - \frac{dy_{1-}}{dt}\right), \quad \frac{dy_{2+}}{dt} = \frac{dy_{2-}}{dt}$$
$$\text{if } |x-y_2| = b2$$
$$\frac{dx_+}{dt} - \frac{dy_{2+}}{dt} = -R\left(\frac{dx_-}{dt} - \frac{dy_{2-}}{dt}\right), \quad \frac{dy_{1+}}{dt} = \frac{dy_{1-}}{dt}$$

¹⁰¹ The subscripts $+$ and $-$ indicate time immediately after and before impacts.

5

102 *R* represents the restitution coefficient of impact. The dimensionless variables as
103 follows are introduced:

$$
\begin{aligned}
&\omega^2 = \frac{K}{M}, \quad T = \omega t, \quad \lambda = \frac{C}{(m_1+m_2)\omega}, \quad \varepsilon = \frac{m_1+m_2}{M}, \\
&G = \frac{F}{(m_1+m_2)\omega^2}, \quad X = \frac{x}{b1}, \quad Y_1 = \frac{y_1}{b1}, \\
&Y_2 = \frac{y_2}{b1}, \quad \Delta = \frac{b2}{b1}, \quad \alpha_i = \frac{m_i}{m_1+m_2}, \quad \tilde{\Omega} = \frac{\Omega}{\omega}
\end{aligned}
\tag{3}
$$

104 After substitution of Eq.(3) in Eq.(1), it becomes:

$$
\begin{aligned}
&\ddot{x} + \varepsilon\lambda\dot{X} + X = \varepsilon G \sin\tilde{\Omega}T, \\
&\varepsilon\alpha_1\ddot{Y}_1 = 0, \\
&\varepsilon\alpha_2\ddot{Y}_2 = 0, \forall |X-Y_1| < 1 \text{ and } |X-Y_2| < \Delta
\end{aligned}
\tag{4}
$$

105 In the same way, after substitution of Eq.(3) in Eq.(2), it becomes:

$$
\begin{aligned}
&\forall |X-Y_1| = 1 \quad \text{or } |X-Y_2| = \Delta \\
&X_+ = X_-, \quad Y_{1+} = Y_{1-}, \quad Y_{2+} = Y_{2-} \\
&M\dot{X}_+ + \varepsilon\alpha_1\dot{Y}_{1+} + \varepsilon\alpha_2\dot{Y}_{2+} = M\dot{X}_- + \varepsilon\alpha_1\dot{Y}_{1-} + \varepsilon\alpha_2\dot{Y}_{2-} \\
&\text{if } |X-Y_1| = 1 \quad \dot{X}_+ - \dot{Y}_{1+} = -R\left(\dot{X}_- - \dot{Y}_{1-}\right), \quad \dot{Y}_{2+} = \dot{Y}_{2-} \\
&\text{ifi } |X-Y_2| = \Delta \quad \dot{X}_+ - \dot{Y}_{2+} = -R\left(\dot{X}_- - \dot{Y}_{2-}\right), \quad \dot{Y}_{1+} = \dot{Y}_{1-}
\end{aligned}
\tag{5}
$$

106 The barycentric coordinates are introduced in the following way:

$$
V = X + \varepsilon\alpha_1 Y_1 + \varepsilon\alpha_2 Y_2, \quad W_1 = X - Y_1, \quad W_2 = X - Y_2
\tag{6}
$$

107 These coordinates correspond to the physical displacement of the center of
108 mass and the relative displacement of VI NES. The substitution of Eq.(6) in Eq.(4)
109 and Eq.(5) gives:

6

$$\ddot{V} + \frac{V + \varepsilon\alpha_1 W_1 + \varepsilon\alpha_2 W_2}{1+\varepsilon} + \varepsilon\lambda \frac{\dot{V} + \varepsilon\alpha_1 \dot{W}_1 + \varepsilon\alpha_2 \dot{W}_2}{1+\varepsilon}$$

$$= \varepsilon G \sin\tilde{\Omega}T$$

$$\ddot{W}_1 + \frac{V + \varepsilon\alpha_1 W_1 + \varepsilon\alpha_2 W_2}{1+\varepsilon} + \varepsilon\lambda \frac{\dot{V} + \varepsilon\alpha_1 \dot{W}_1 + \varepsilon\alpha_2 \dot{W}_2}{1+\varepsilon}$$

$$= \varepsilon G \sin\tilde{\Omega}T \tag{7}$$

$$\ddot{W}_2 + \frac{V + \varepsilon\alpha_1 W_1 + \varepsilon\alpha_2 W_2}{1+\varepsilon} + \varepsilon\lambda \frac{\dot{V} + \varepsilon\alpha_1 \dot{W}_1 + \varepsilon\alpha_2 \dot{W}_2}{1+\varepsilon}$$

$$= \varepsilon G \sin\tilde{\Omega}T$$

$$\forall |W_1| < 1 \text{ and } |W_2| < \Delta$$

$$\forall |W_1| = 1 \quad \text{or } |W_2| = \Delta$$

$$V_+ = V_-, \quad W_{1+} = W_{1-},$$

$$W_{2+} = W_{2-}, \quad \dot{V}_+ = \dot{V}_-$$

$$\text{if } |W_1| = 1$$

$$\dot{W}_{1+} = -R\dot{W}_{1-}, \quad \dot{W}_{2+} = \dot{W}_{2-} - \frac{\varepsilon\alpha_1(1+R)}{1+\varepsilon\alpha_1}\dot{W}_{1-} \tag{8}$$

$$\text{if } |W_2| = \Delta$$

$$\dot{W}_{2+} = -R\dot{W}_{2-}, \quad \dot{W}_{1+} = \dot{W}_{1-} - \frac{\varepsilon\alpha_2(1+R)}{1+\varepsilon\alpha_2}\dot{W}_{2-}$$

[110] Eqs.(7) and (8) are analyzed with the multiple scales method. Solutions are
[111] found in the following form:

$$V(T_0, T_1) = V_0(T_0, T_1) + \varepsilon V_1(T_0, T_1) + \dots$$

$$W_1(T_0, T_1) = W_{10}(T_0, T_1) + \varepsilon W_{11}(T_0, T_1) + \dots \tag{9}$$

$$W_2(T_0, T_1) = W_{20}(T_0, T_1) + \varepsilon W_{21}(T_0, T_1) + \dots$$

[112] with $T_i = \varepsilon^i T$. After substitution of Eq.(9) in Eq.(7) and Eq.(8), they become
[113] as follows:

7

114   • Ordre ε^0

$$
\begin{aligned}
&\forall |W_{10}| < 1 \text{and } |W_{20}| < \Delta \\
&D_0^2 V_0 + V_0 = 0, \\
&D_0^2 W_{10} + V_0 = 0, \quad D_0^2 W_{20} + V_0 = 0 \\
&\forall |W_{10}| < 1 \text{or } |W_{20}| < \Delta \\
&V_{0+} = V_{0-}, \quad W_{10+} = W_{10-}, \\
&W_{20+} = W_{20-}, \quad D_0 V_{0+} = D_0 V_{0-} \\
&\text{if } |W_{10}| = 1 \\
&D_0 W_{10+} = -R D_0 W_{10-}, \quad D_0 W_{20+} = D_0 W_{20-} \\
&\text{if } |W_{20}| = \Delta \\
&D_0 W_{20+} = -R D_0 W_{20-}, \quad D_0 W_{10+} = D_0 W_{10-}
\end{aligned}
\tag{10}
$$

115   • Ordre ε^1

$$
\begin{aligned}
D_0^2 V_1 + V_1 &= -\alpha_1 W_{10} - \alpha_2 W_{20} \\
&+ V_0 - 2 D_0 D_1 V_0 - \lambda D_0 V_0 + G \sin \Omega T_0
\end{aligned}
\tag{11}
$$

116   The solution of the first equation of Eq.(10) can be written in the following
117   way:

$$
V_0(T_0, T_1) = A(T_1) \sin(T_0 + \alpha(T_1))
\tag{12}
$$

118   The second and third equation of Eq.(10) represent an oscillator with vibro-
119   impacts under periodic excitations. Like in [29], Their solutions can be expressed
120   with standard trigonometric functions as follows:

$$
\begin{aligned}
W_{j0}(T_0, T_1) &= A(T_1) \sin(T_0 + \alpha(T_1)) \\
&+ \frac{2B_j}{\pi} \arcsin(\cos(T_0 + \eta_j(T_1))), \quad j = 1, 2
\end{aligned}
\tag{13}
$$

8

¹²¹ Combined with the conditions of impacts given in Eq.(10), the following rela-
¹²² tions are obtained:

$$
\begin{aligned}
\sin(\alpha - \eta_1) &= \frac{1 - B_1}{A}, \quad \cos(\alpha - \eta_1) = \frac{2B_1\delta}{A\pi} \\
\sin(\alpha - \eta_2) &= \frac{\Delta - B_2}{A}, \quad \cos(\alpha - \eta_2) = \frac{2B_2\delta}{A\pi}
\end{aligned}
\tag{14}
$$

¹²³ with $\delta = (1 - R)/(1 + R)$, these relations can be combined through using the
¹²⁴ trigonometric identity:

$$
A^2 = (1 - B_1)^2 + \frac{4B_1^2\delta^2}{\pi^2} = (\Delta - B_2)^2 + \frac{4B_2^2\delta^2}{\pi^2}
\tag{15}
$$

¹²⁵ Eq.(15) represents one algebraic relation related to the displacement amplitude
¹²⁶ of LO and that of two VI NES, which is termed as SIM. In the first approximation
¹²⁷ order, the amplitude of every VI NES only depends on the amplitude of the main
¹²⁸ system and the performance of two VI NES is decoupled. It establishes the ana-
¹²⁹ lytical foundation of the principle of separate activation as stated in [42, 43] for
¹³⁰ the case of cubic NES, which is also applicable for VI NES here.

¹³¹ Eq.(11) in the order ε^1 is now studied. To identify secular terms, the solutions
¹³² of W_{j0} are developed in series of Fourier. The development for one harmonic
¹³³ gives:

$$
W_{j0} = A\sin(T_0 + \alpha) + \frac{8B_j}{\pi^2}\cos(T_0 + \eta_j), \quad j = 1, 2
\tag{16}
$$

¹³⁴ The system is studied in the vicinity of the resonance frequency of the main
¹³⁵ system. The pulsation of excitation is expressed in the following way:

$$
\tilde{\Omega} = 1 + \varepsilon\sigma
\tag{17}
$$

9

136   After the substitution of Eqs.(12, 16) and Eq.(17) in Eq.(11), it comes:

$$
\begin{aligned}
D_0^2 V_1 + V_1 \\
= -\sum_{j=1}^2 \left[\alpha_j \left(A\sin(T_0+\alpha) + \frac{8B_j}{\pi^2}\cos(T_0+\eta_j) \right) \right] \\
-2D_1 A\cos(T_0+\alpha) + A\sin(T_0+\alpha)(1+2D_1\alpha) \\
-\lambda A\cos(T_0+\alpha) + G\sin(T_0+\sigma T_1)
\end{aligned}
\tag{18}
$$

137   After arrangement, the condition for the elimination of secular term is as fol-
138 lows:

$$
\begin{aligned}
2D_1 A &= -\sum_{j=1}^2 \left[\frac{8\alpha_j B_j}{\pi^2}\cos(\alpha-\eta_j) \right] - \lambda A + G\sin(T_1\sigma-\alpha) \\
2AD_1\alpha &= \sum_{j=1}^2 \left[\frac{8\alpha_j B_j}{\pi^2}\sin(\alpha-\eta_j) \right] - G\cos(T_1\sigma-T_1)
\end{aligned}
\tag{19}
$$

139   The expressions of $\sin(\alpha-\eta_j)$ and $\cos(\alpha-\eta_j)$ $(j=1,2)$ given in Eq.(14) are
140 substituted in Eq.(19), then the change of variable $T_1\sigma-\alpha=\theta$ is introduced:

$$
\begin{aligned}
2D_1 A &= \frac{16\alpha_1 B_1^2 \delta}{\pi^3 A} - \frac{16\alpha_2 B_2^2 \delta}{\pi^3 A} - \lambda A + G\sin\theta \\
2AD_1\theta &= -\frac{8\alpha_1 B_1(1-B_1)}{A\pi^2} - \frac{8\alpha_2 B_2(\Delta-B_2)}{A\pi^2} + G\cos\theta + 2A\sigma
\end{aligned}
\tag{20}
$$

141   The fixed points to the limit $T_1 \to \infty$ are calculated by eliminating the deriva-
142 tion in Eq.(20). The obtained equations can be combined by using the trigonomet-
143 ric identity. After rearrangement, one equation of the following form is obtained:

$$
c_2 A^4 + c_1(B_1,B_2)A^2 + c_0(B_1,B_2) = 0
\tag{21}
$$

144   Eq.(21) can be expressed in the function of only A and B_1 or B_2 by using
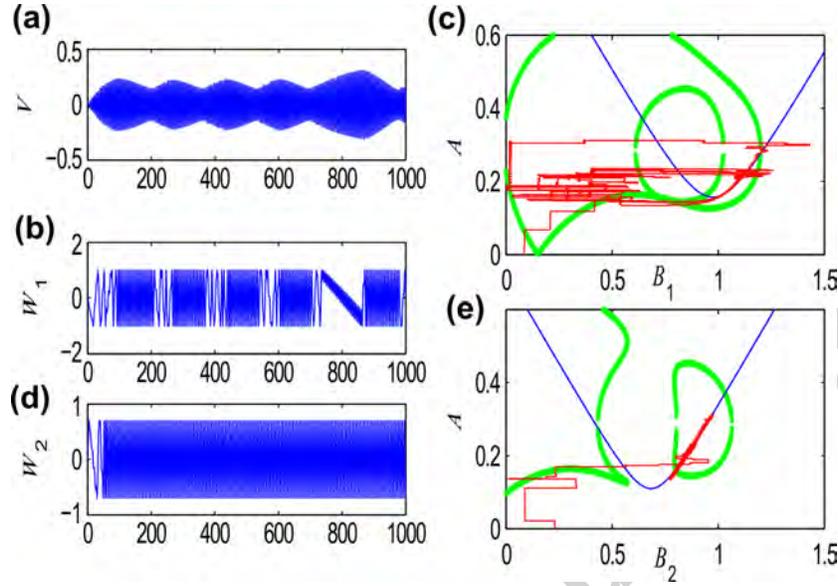145 Eq.(15). The obtained equation can be resolved for A^2.

10

Fig. 2. Numerical integration of Eqs. (7, 8) for $G = 0.8$ and $\sigma = 0.5$: (a) SMR of V; (b) intermittent resonance of W_1 related to the first VI NES; (c) the analytically obtained SIM of the first order in blue curve and of the second order in green curve, the projection of motion for the first VI NES in red curve; (d) the constant response of W_2 related to the second VI NES; (e) the projection of motion for the second VI NES in red curve.

¹⁴⁶   The thereby obtained algebraic relation between A and B_1 or B_2 represents the

¹⁴⁷ invariant manifold of the problem in the time-scale T_1. Subsequently, different

¹⁴⁸ results of numerical integration and their projections into the invariant manifold

¹⁴⁹ of each VI NES are presented.

¹⁵⁰ 3. Numerical results

¹⁵¹   In this part, the objective is to validate the analytical results by numerical

¹⁵² simulations. The Eqs.(7) and (8) will be used. The used parameters are showed
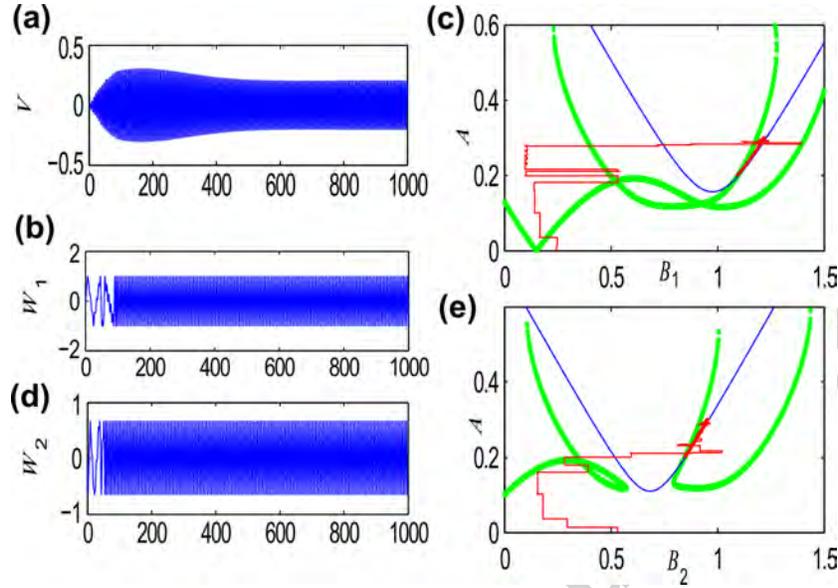
¹⁵³ as follows:

11

Fig. 3. Numerical integration of Eqs. (7, 8) for $G = 0.9$ and $\sigma = -0.2$: (a) steady state response of V; (b) constant resonance of W_1 related to the first VI NES; (c) the analytically obtained SIM of the first order in blue curve and of the second order in green curve, the projection of motion for the first VI NES in red curve; (d) the constant response of W_2 related to the second VI NES; (e) the projection of motion for the second VI NES in red curve.

$$\varepsilon = 0.01, \quad \Delta = 0.7, \quad R = 0.6,$$
$$\alpha_1 = \alpha_2 = 0.5, \quad \lambda = 1$$

(22)

154   The numerical integration results with SIM for $G = 0.8$ and $\sigma = 0.5$ are pre-
155 sented in Fig. 2. In this case, the time history of V, which is an approximate
156 description of the displacement of LO, illustrates its strongly modulated feature
157 [31, 34] as displayed in Fig. 2(a). Its amplitude is chaotic strongly modulated
158 and the relative maximal amplitude is not constant every time. In Fig. 2(b), the
159 relative displacement related to VI NES 1 is showed. The dense parts denote that

12

160 it realizes two impacts per cycle, and the sparse parts denote the occasional out of

161 activation. Therefore, VI NES1 realizes intermittent response . Then, its response

162 is projected to the SIM in red curve as showed in Fig. 2(c). The intersections

163 of the blue curve and the green curve denote the fixed points, but their stabilities

164 are not calculated here. The overlapping parts between the blue curve and the

165 red curve demonstrate the parts with two impacts per cycle and validate the pre-

166 diction accuracy of SIM. For VI NES 2, it is activated in permanence with two

167 impacts per cycle as showed by W_2 in Fig. 2(d). Its motion is projected to SIM

168 as showed in Fig. 2(e), and the projected A and B_2 are always in right branch

169 of SIM. It means that the displacement amplitude of VI NES 2 will always vary

170 simultaneously with that of LO.

171 Another case is presented in Fig. 3 for $G = 0.9$ and $\sigma = -0.2$. In this case,

172 the two VI NES are attracted by fixed points, namely the intersections between

173 the blue curve and red curve, as showed in Fig. 3 (c) and (e). The main system

174 performs steady oscillation as displayed in Fig. 3 (a). Compared to the last case,

175 the values of A, B_1 and B_2 are constant and well predicted by the SIMs.

176 Actually, the ability of SIM obtained by analytical study is limited on predict-

177 ing the resonance responses with two impacts per cycle of main system or other

178 response regimes with resonant parts. Other more complicated phenomena will

179 be demonstrated by the following experimental study.

180 4. Experimental results

181 In this section, experiments are done for periodic and transient excitation re-

182 spectively to compare the case with one VI NES and that with two VI NES. For pe-

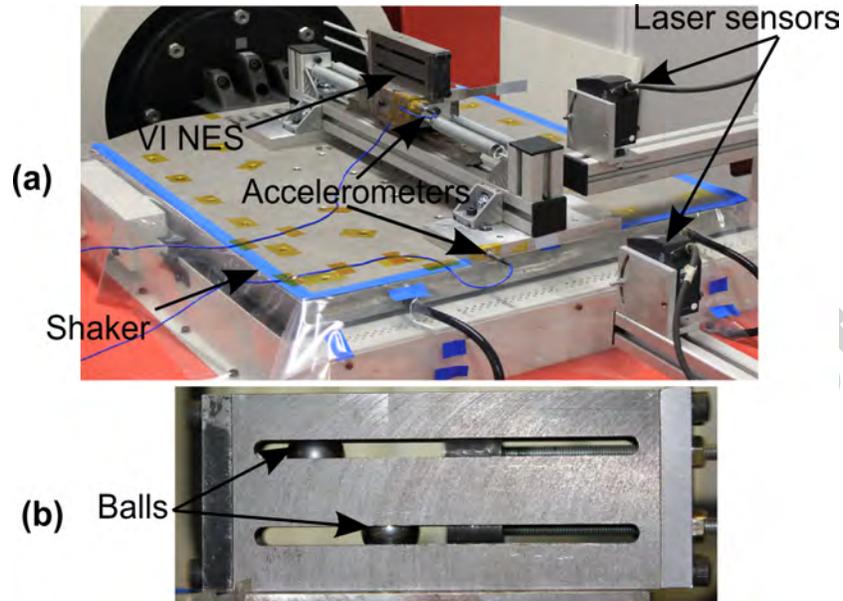183 riodic excitation, the experimentally obtained and used parameters are displayed

13

Fig. 4. Experimental setup: (a) global configuration; (b) detailed view of VI NES.

at the first place. Then, the results under excitation with a single frequency and a range of frequency around resonance frequency are demonstrated to show the possible response regimes, and to compare the efficiency under different combinations of length of cavity. Regarding transient excitation, the same experimental device is applied and the objective is to verify the principle of separate activation.

4.1. Periodic excitation

4.1.1. Experimental setup

The global experimental configuration is showed in Fig. 4(a). Two VI NES are put inside two clearances of LO in parallel as demonstrated in Fig. 4 (b), and they can move freely inside. The whole system is embedded on an electrodynamic shaker with a maximal force 10 kN. The displacement of LO as well as the im-

14

Table 1. Experimental parameters

Physical Parameters			
M	4.7 kg	C	3.02 Ns/m
K	$11.47 \cdot 10^3$ N/m		
m_1	32 g	m_2	32 g
b_1	$0 - 50$ mm	b_2	$0 - 50$ mm
Reduced Parameters			
ε	0.76%	λ_1	1.91
f_0	7.86 Hz		
Single frequency test			
f_r		$7.82 - 7.84$ Hz	
Shaker acceleration		0.06 g	
Frequency band test			
$f_s - f_e$		$6.5 - 9$ Hz	
Shaker acceleration		0.06 g	

15

posed displacement of the shaker are measured by contact-less laser displacement sensors. Their accelerations are measured by accelerometers and the impacts between VI NES and LO can be judged from the sudden changes of the acceleration of LO. A detailed view of the configuration for two VI NES is presented in Fig. 4 (b). It simply consists of two closed clearances of lengths $d + 2 \cdot b1$ and $d + 2 \cdot b2$, respectively, where d is the diameter of both balls (VI NES). $b1$ and $b2$ are lengths of the above clearance and the below clearance, respectively, and each can be adjusted by a cylinder. The cylinder and the cover at the opposite side are made of hardened steel. The parameters of this system have been identified by performing modal analysis and are summarized in Table 1.

4.1.2. Single frequency excitation

The frequency of the sinusoidal excitation is slowly varied from 7.82 Hz to 7.84 Hz during 80 s, which can be considered almost fixed to the value 7.83 Hz. This value is closed to the natural frequency of LO ($f_0 = 7.86$ Hz). The acceleration of the shaker is fixed to 0.06 g. During the whole experimental process, the time histories of displacement and acceleration of LO are recorded.

With the change of the number of VI NES and different combinations of clearances b1 and b2, different periodic and transient response regimes are observed and demonstrated here. They are identified by the difference of impact numbers per cycle of LO, which can be judged from the time history of the acceleration of LO.

At first, the time history of the acceleration of LO without VI NES is showed in Fig. 5(a) as a reference. Although there exist small shakes at some of its maximal place, no impacts exist. In addition, its amplitude is highest compared to other cases coupled with VI NES. Then, the time history of the acceleration of LO with

16

a VI NES for a clearance of 30 mm is showed in Fig. 5(b) as another reference. This value of clearance is proved to be almost optimal in the sense of vibration control and the response regime is two impacts per cycle [36]. It is not so easy to distinguish impacts because the order of impact strength is close to that of the acceleration of LO, but the impact number is observable during the process of experiment. Moreover, the peaks of acceleration are evidently reduced compared to the results in Fig. 5(a).

With the addition of another ball and different combinations of clearances, the response regimes will be more complicated. However, the possible variations are always based on the above two cases. Then, the regime with four impacts per cycle is observed with the addition of a second ball with clearance $b1 = 5$ mm (another ball with clearance $b2 = 30$ mm), and both ball impact twice per cycle as showed in Fig. 5(c), and the four impact moments during one cycle are marked out in rectangles. The acceleration of LO is further decreased compared to the optimized one ball case with 30 mm clearance, and this efficiency improvement cannot be easily judged here and will be demonstrated from the viewpoint of displacement later.

When the clearance of the added ball is increased to 40 mm, the response is complicated as displayed in Fig. 5(d). The ball below with $b2 = 30$ mm continuously impacts twice per cycle. In contrast, the added ball impacts only once during many cycles (> 1), and a few of them are marked out in rectangles.

In addition to the above relative stable response regimes, there exist some even more complicated transient response regimes during one time history for some combinations of clearances. For the case with $b1 = b2 = 30$ mm, there are some periods as showed in Fig. 5(e), in which just one ball is activated with two
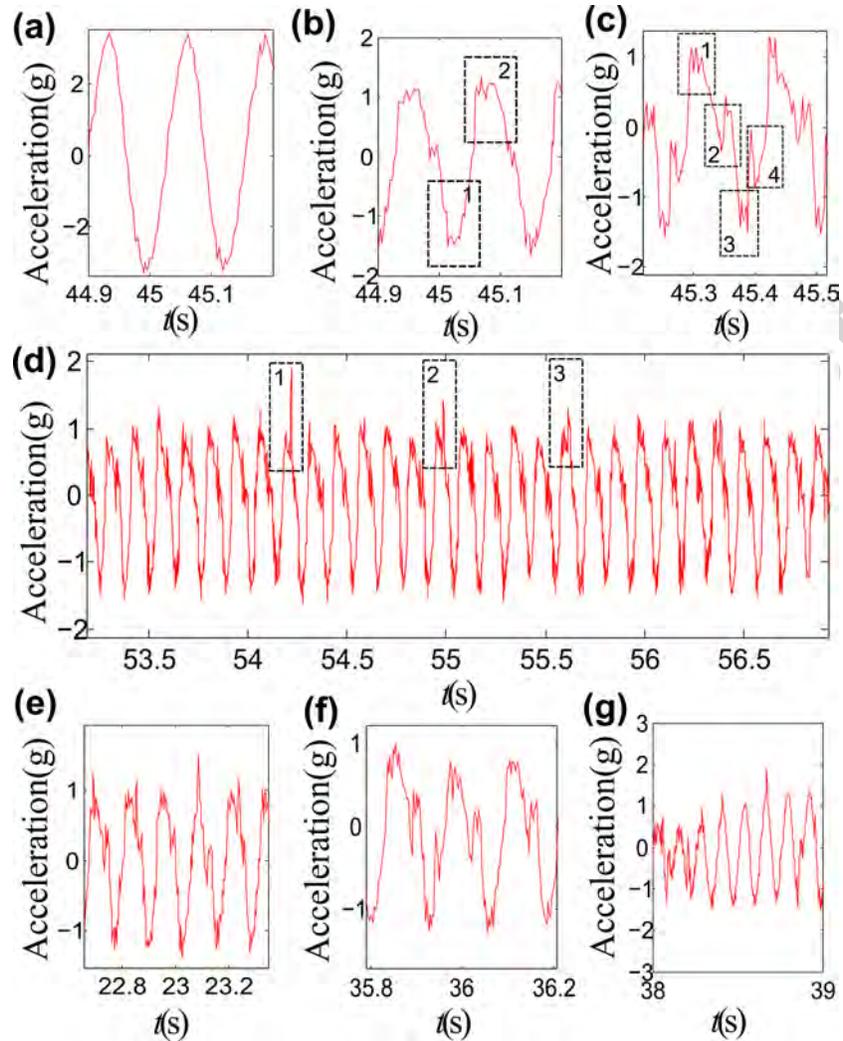
17

Fig. 5. Typical response regimes by comparison of impact numbers per cycle of the acceleration of LO and some impacts moments are marked out in rectangle: (a) no impact and no VI NES; (b) two impacts per cycle; (c) four impacts per cycle; (d) one VI NES impacts once during many cycles and another VI NES impacts twice per cycle; (e) one period of a response with at least one VI NES in the state of two impacts per cycle; (f) one period of a response with both VI NES in the state of two impacts per cycle; (g) one period of a response with both VI NES out of activation and no impact.

18

impacts per cycle, but this activated state can alternate between these two balls.
This phenomenon is complicated, and it cannot be judged from the results showed
here and can just be observed in the test site. There are also some periods, two
balls impact twice per cycle as showed in Fig. 5(f) and there are even some periods
there are almost no impacts as showed in Fig. 5(g).

Therefore, the strong nonlinear coupling between these two balls and LO is
well observed by the complicated variations of response regimes during one time
history. The above mentioned basic response regimes will be applied to explain
the complication variation of efficiency, and this point is closely related to the
targeted energy transfer by transient resonance captures.

In [36], it is observed that the optimal response regime is the one with two im-
pacts per cycle and around the entrance of SMR. The idea of optimization design
is to make efficient response regimes occur for different excitations. This idea can
still apply in the optimization design of two VI NES, namely to make each VI
NES activated at its best state with two impacts per cycle.

Then, the efficiency comparison of different combinations of clearances is per-
formed here to observe the possible relation between the types of response regimes
and their efficiency. The two cases without VI NES and with one optimized VI
NES (30 mm clearance) are chosen as two references as showed in Fig. 6(a-b).

The length of the down clearance $b2$ is fixed to 30 mm and only the upper
clearance $b1$ is varied from 5 mm to 50 mm. Here, only the time histories of
displacement are demonstrated for $b1 = 30$ mm and $b1 = 5$ mm, respectively.
The former is displayed in Fig. 6(a), there are three typical areas A1, A2 and
A3, which correspond to typical response regimes from Fig. 5(e) to Fig. 5(g),
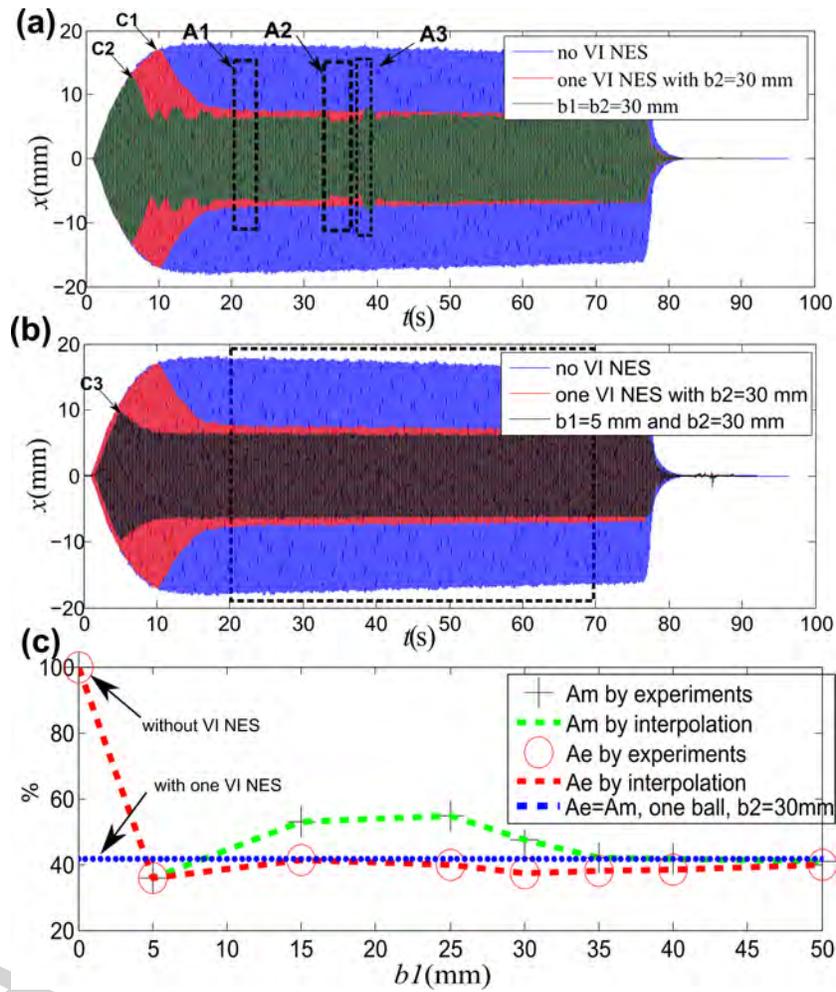respectively. In area A1, there is a small decrease of amplitude compared to the

19

Fig. 6. Typical response regimes and their efficiency comparison with different combinations of clearances: (a-b) response regimes; (c) efficiency comparison by average and maximal amplitude ratios (Ae and Am).

270 one VI NES case in red curve. In area A2, both ball impact twice per cycle and the

271 amplitude is lowest. In area A3, the occasional out of activation for both balls and

272 the amplitude increases. In the whole process, there are many transitions between

273 them, which results in the complicated variation of displacement amplitude of LO.

274 It is a direct proof of nonlinear coupling between two VI NES and LO. In addition,

275 the efficiency is highest when both balls impact twice per cycle, which is the most

276 effective form of transient resonance captures.

277   This efficient targeted energy transfer is better demonstrated by the decrease

278 of b1 to 5 mm as showed in Fig. 6(b). This time, both VI NES impact twice per

279 cycle and it means the permanent resonance captures.

280   With the excitation of LO at the beginning, different activation amplitudes of

281 LO with different combinations of clearances are observed, namely C1, C2 and C3

282 in Fig. 6(a-b). With the increase of VI NES from 0 to 1, and then 2, the amplitude

283 is evidently decreased at the activation point of VI NES. The same conclusion

284 is obtained when the value of another clearance is decreased. In this sense, the

285 robustness and efficiency can be improved.

286   Then, the average and maximal amplitude ratios between the case with VI

287 NES and without NES are calculated for all cases during a stable time period (20-

288 70 s), and the results are showed in Fig. 6(c). Compared to the case without VI

289 NES and with one VI NES, the optimal case is the addition of another VI NES

290 with a small clearance 5 mm. For other cases with large clearances, it cannot im-

291 prove the efficiency and, in return, it will result in the occasional out of activation

292 of VI NES, and meanwhile, the large displacement of LO.

293   According to the optimization design criterion proposed in [36], the design

294 of parameters is to make the efficient response regimes appear and it means the

21

295 most efficient transfer and dissipation of energy. From the above experimental

296 results with limited combinations of clearances, this optimization design criterion

297 still applies since both balls impacts twice in the optimal case with $b1 = 5$ mm.

298 However, the phase difference of two VI NES cannot be measured or calculated,

299 it may be another factor related to efficiency.

300 Except the above combinations of clearances, experiments with the same clear-

301 ance for both VI NES are also performed. The average and maximal amplitude

302 ratios are also calculated and showed in Fig. 7. From the viewpoint of Ae, the case

303 with $b1 = b2 = 30$ mm is optimal. On the contrary, the case with $b1 = b2 = 15$

304 mm is optimal in terms of Am. Generally speaking, they are less effective than

305 the combination with $b1 = 5$ mm and b2=30 mm.

306 As a summary, the objective to find the relation between response regimes

307 and their efficiency is accomplished in two steps. The first step is to find basic

308 response regimes. Then, they are applied to explain the complicated variation of

309 response. As a result, a general design criterion can also be proposed here: the

310 design of two VI NES is to make them activated around most efficient response

311 regimes.

312 *4.1.3. Excitation with a band of frequency*

313 Then, the band of excitation frequency is enlarged around the natural fre-

314 quency of LO. The objective here is to study the influence of different combi-

315 nations of clearances on the response regimes and their efficiency. The starting

316 frequency f_s and ending frequency f_e during this sweep is showed in Table 1 and

317 the acceleration is still fixed to 0.06 g.

318 For the above experimental configuration, the one VI NES case with a clear-

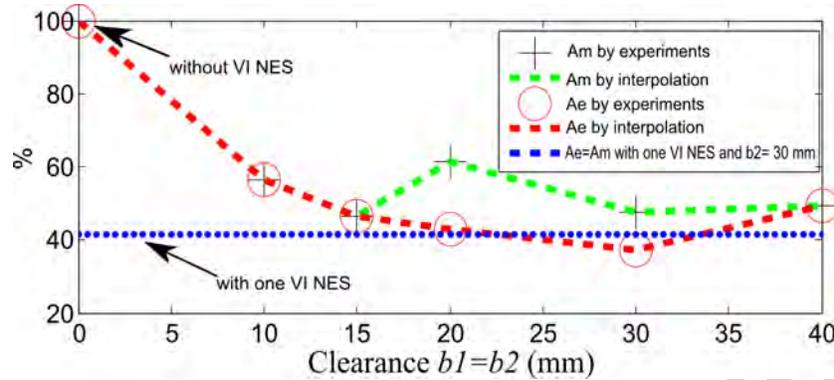319 ance 27.5 mm has been observed optimal [36]. Here the clearance of an added

22

Fig. 7. Efficiency comparison of different response regimes with the same clearance for both VI NES.

³²⁰ VI NES is selected around this value. The displacement of LO is recorded for
³²¹ different combinations of $b1$ and $b2$ and is showed in Fig. 8. The results with
³²² fixed $b2 = 27.5$ mm and varying $b1$ are showed in Fig. 8(a). The combination of
³²³ $b1 = 12.5$ mm and $b2 = 27.5$ mm is generally more optimal in this case. Then,
³²⁴ the results with equal $b1$ and $b2$ are showed in Fig. 8(b). For frequencies a little
³²⁵ below the resonance frequency, the combination of $b1 = 27.5$ mm and $b2 = 27.5$
³²⁶ mm is better, but the other two are better for frequencies a little higher than the
³²⁷ resonance frequency. To have a close view, the results between two relative op-
³²⁸ timal cases are compared in Fig. 8(c). In area A, it is observed that VI NES can
³²⁹ be activated at a lower value of displacement amplitude for a smaller $b1$. In area
³³⁰ B, two VI NES are in regime with two impacts per cycle for $b1 = 27.5$ mm. On
³³¹ the contrary, one ball occasionally gets out of activation for $b1 = 12.5$ mm and
³³² results in the transient build-up of amplitude. In area C, low $b1 = 12.5$ mm still
³³³ can be activated for lower amplitude and results in the reduction of amplitude. As
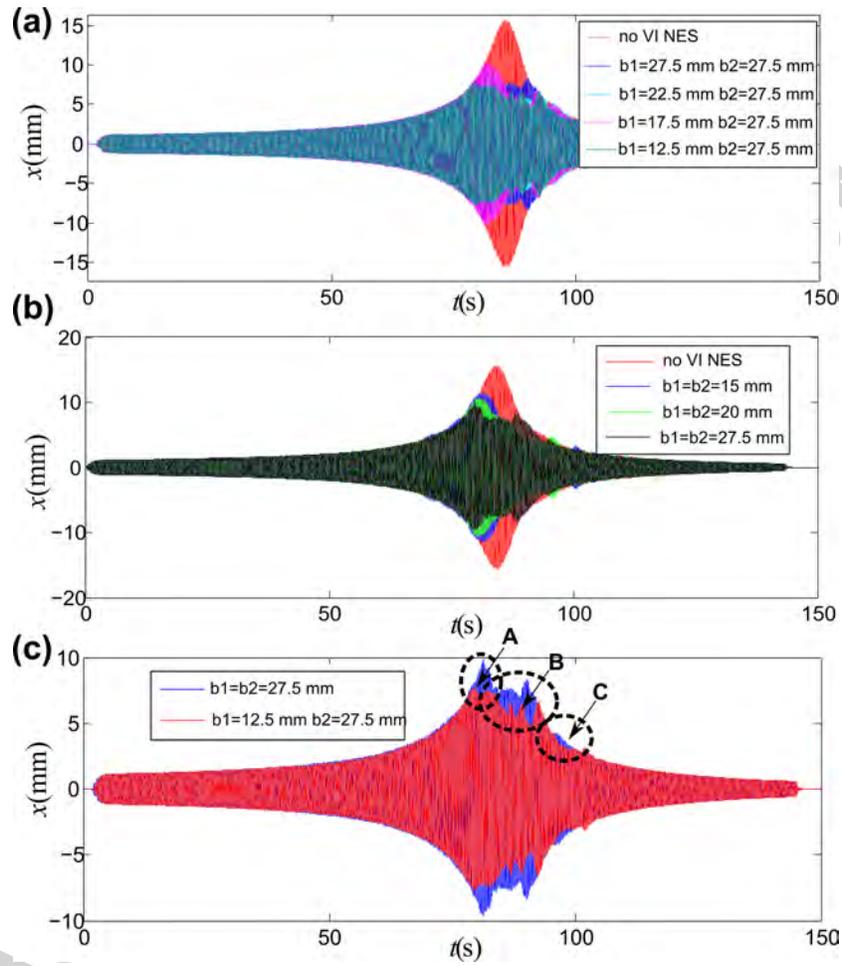³³⁴ has been demonstrated under the excitation with a fixed frequency, the variation

23

Fig. 8. Responses of LO during the sweep experiments and efficiency comparison: (a) with different $b1$ and $b2$; (b) with the same $b1$ and $b2$; (c) the efficiency comparison for two relative optimal cases.
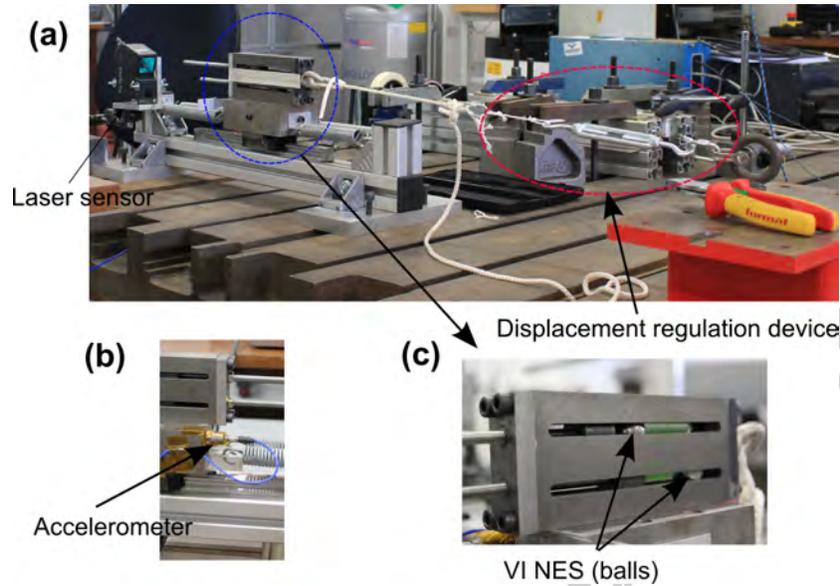
Fig. 9. Experimental setup: (a) global configuration; (b) installation of accelerometer; (c) detailed view of VI NES.

of motion for LO and both VI NES can be more complicated than the above-mentioned characteristics. Except the observed relation between efficiency and the response regimes, it is desirable to obtain further information but this kind of try would be difficult.

Therefore, the following optimization design criterion is recommended. If just one ball is applied, it is recommended that VI NES should be optimized at the point of natural frequency. If two VI NES are applied to improve the robustness and increase efficiency, a smaller length of clearance should be chosen compared to the optimized clearance of the one ball case to avoid the occasional failure.

₃₄₄ *4.2. Transient excitation*

₃₄₅ *4.2.1. Experimental setup*

₃₄₆   The same experimental device as the periodic case is used, but it is attached to
₃₄₇ a cast iron bench as showed in Fig. 9(a). The addition of a small ring bolt for pre-
₃₄₈ stretch will not influence the total mass of LO and its influence can be neglected.
₃₄₉ Therefore, its parameters are nearly the same as these in Table 1. One laser sen-
₃₅₀ sor and one accelerometer are used to measure the displacement and acceleration
₃₅₁ of LO, respectively. The fixation of accelerometer is showed in Fig. 9(b) and a
₃₅₂ detailed view of VI NES is displayed in Fig. 9(c). The number of balls can be
₃₅₃ changed. The initial displacement of LO is regulated by a device and is fixed to
₃₅₄ 20 mm for all tests. The initial location of two balls are at random, and the ve-
₃₅₅ locities for LO and both balls are zero. Since only the stable transition process is
₃₅₆ studied and the transient process quickly disappears, the initial conditions will not
₃₅₇ influence the expected conclusion.

₃₅₈ *4.2.2. Principle of separate activation*

₃₅₉   With two sets of $b1$ and $b2$, the responses of two cases are compared here. For
₃₆₀ the case with one VI NES ($b2 = 20$ mm), the time history of displacement of LO
₃₆₁ is represented by the red curve in Fig. 10(a) and its corresponding acceleration is
₃₆₂ showed in Fig. 10(b). The points A1 and A2 are related to the transition from the
₃₆₃ regime with two impacts per cycle to that without any continuous period of two
₃₆₄ impacts per cycle.

₃₆₅   For the case with two balls ($b1 = 2$ mm and $b2 = 20$ mm), the time history
₃₆₆ of displacement of LO is represented by the blue curve in Fig. 10(a) and its cor-
₃₆₇ responding acceleration is showed in Fig. 10(c). The first VI NES with $b2 = 20$
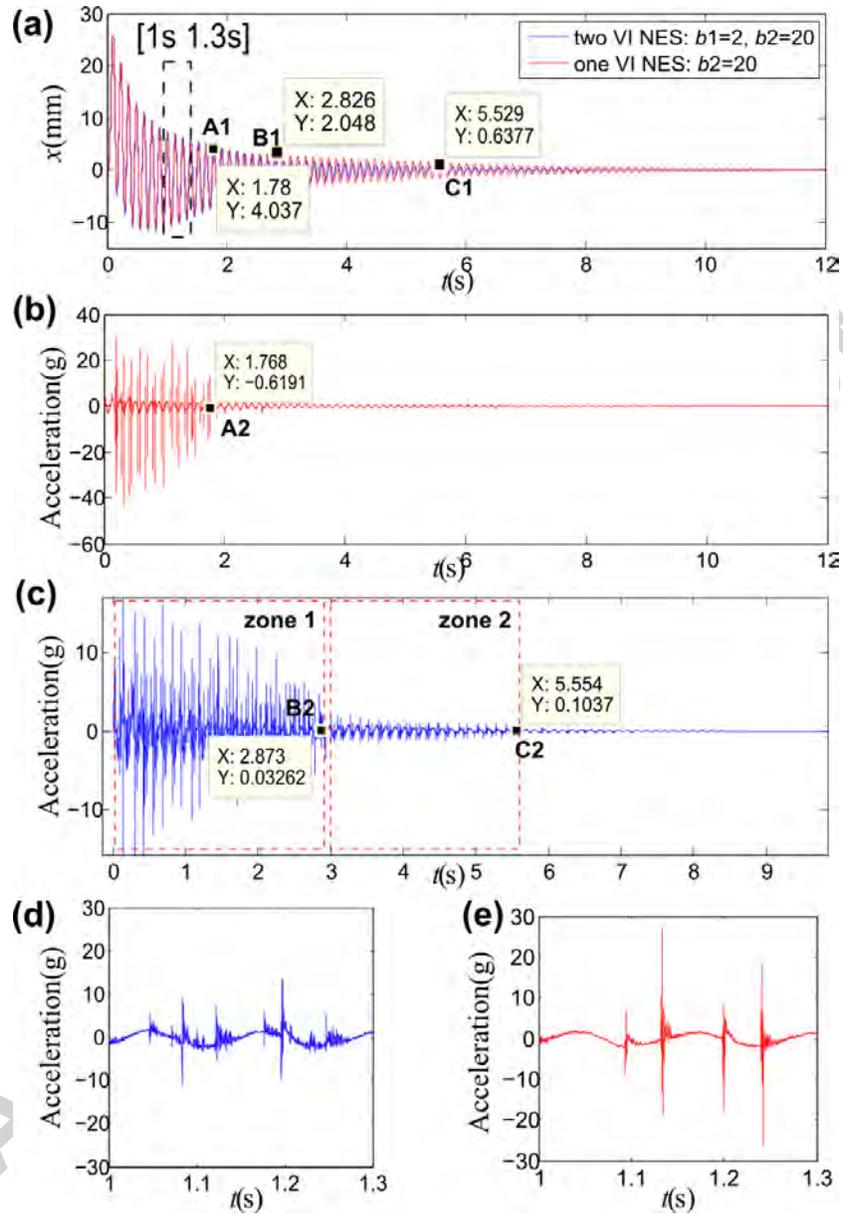₃₆₈ mm gets out of two impacts per cycle around points B1 and B2. The second VI

26

Fig. 10. Response comparison between LO coupled with one VI NES and two VI NES: (a) an imposed time history of displacement; (b) a time history of acceleration with one VI NES; (c) a time history of acceleration with two VI NES; (d) a detailed view of one period of acceleration with two VI NES; (e) a detailed view of one period of acceleration with one VI NES.

27

369 NES with a small clearance $b1 = 2$ mm gets out of two impacts per cycle around

370 points C1 and C2. In zone 1, the first VI NES with a large clearance is activated

371 with two impacts per cycle. In zone 2, the first VI NES gets out of activation and

372 the second VI NES with a small clearance is activated with two impacts per cycle.

373 In the sense of the activation with two impacts per cycle, the principle of separate

374 activation of VI NES with different clearances is observed here. This definition

375 of activation is important, since the regime with two impacts per cycle is most

376 efficient in vibration control [36].

377 Then, the decay rates of displacements for both cases are compared. Before

378 point A1, there is almost no difference, since the first VI NES with large clearance

379 is activated with two impacts per cycle and the second VI NES behaves in low

380 efficient regime (more than two impacts per cycle). Between A1 and B1, the role

381 of the second VI NES increases but still small. In contrast, it plays an important

382 role between B1 and C1 since it is activated with two impacts per cycle and the

383 first VI NES is totally out of excitation. The difference of decay rates in this

384 period is relative large. Here, the role of separate activation in vibration control

385 is evident, and the two VI NES with difference clearances can be effective at

386 different ranges of displacement amplitude. More importantly, this effectiveness

387 is related to the efficient response regime with two impacts per cycle.

388 During the above transition process, the first VI NES changes from two im-

389 pacts per cycle to the state with no continuous periods of two impacts per cycle

390 (i.e., permanent out of activation), the limit point is A1. It means that it plays the

391 main role in vibration control before A1. In contrast, the second VI NES changes

392 from more than two impacts per cycle to two impacts per cycle, and finally out of

393 activation, it plays a main role in vibration control between B1 and C1. Between
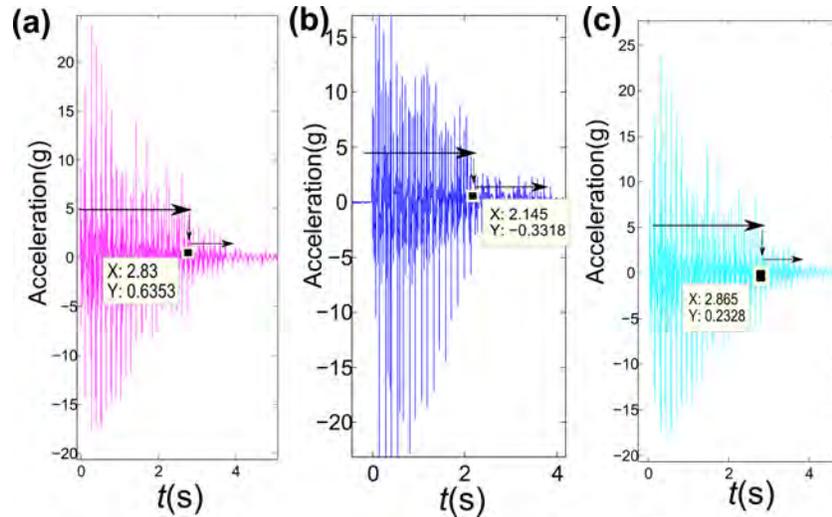
28

Fig. 11. Principle of separate activation: (a) $b1 = 5$ mm and $b2 = 20$ mm; (b) $b1 = 5$ mm and $b2 = 30$ mm; (c) $b1 = 5$ mm and $b2 = 40$ mm.

394 A1 and B1, it is the overlapping period. Evidently, the second VI NES undergoes
395 more response regimes and could possess four impacts per cycle, three impacts
396 per cycle and two impacts per cycle etc., which are closely related to different
397 transient resonance captures.

398   In addition to displacement decay rates, impacts reflected by acceleration can
399 also reveal some important characteristics. The time histories of acceleration of
400 LO from 1 s to 1.3 s are taken out for both cases, as showed in Fig. 10(d) for
401 two VI NES case and in Fig. 10(e) for one VI NES case. With the addition of
402 another ball, the impact strengths are decreased and the impacts are scattered. As
403 observed by other researchers, the regime with strong impact strengths but less
404 impact numbers is replaced by that with weak and more impacts, but the whole
405 energy reduction rate is not improved.

406   The principle of separate activation is also observed from results with other

29

combinations of clearances as showed in Fig. 11. The separate points for the out of activation of the VI NES with a large clearance are marked out in each subfigure. The horizontal arrows demonstrate the two activation levels for two different clearances, and the vertical arrows denote the change between them.

In summary, the principle of separate activation of VI NES is observed, and the effectiveness of the vibration control can be increased to a large range of displacement amplitude of LO. Moreover, the addition of VI NES can reduce impact strengths and scatter impacts though it may not increase the efficiency of vibration control.

5. Conclusion

A LO coupled with two VI NES in parallel is studied under periodic and transient excitations. Firstly, the system is analytically studied with the multiple scales method. SIM is obtained and fixed points can be calculated. Then, numerical simulations are performed to observe the typical response regimes and to validate the analytical results. Finally, experiments under different types of excitations are carried out to observe the possible response regimes and to compare the efficiency of different combinations of clearances.

The asymptotic method, which has been proved feasible for the analytical study of systems coupled with one VI NES, is generalized to the case with two VI NES. Two different SIMs are obtained for two VI NES with different clearances. Since a SIM is related to an activation threshold, namely displacement amplitude of LO, the analytically obtained two different SIMs can explain the principle of separate activation. This principle can be more directly reflected by the transient excitation case. In addition to SIM, fixed points can be calculated and their po-

30

sition can be applied to judge the types of response regimes. Compared to the former analytical methods, the variation of transient and modulated response can be further explained this time. Numerical results prove the consistency of analytical prediction of two classic response regimes, namely two impacts per cycle and SMR. More specifically about SMR, its existence and its periods with two impacts per cycle can be well predicted by SIM.

Although analytical study is limited to obtain results for regimes with two impacts per cycle and SMR, or any combinations of these two regimes, they are still important. From the viewpoint of TET by resonance captures, these regimes possess the most efficient permanent or transient resonance captures.

Through experiments under different excitations, different response regimes are observed and their relation to their efficiency is analyzed. Whatever types of excitation, it is more effective as long as the two VI NES are activated with two impacts per cycle or around this regime. In addition to this common law, the results are complicated from the viewpoint of each excitation type. This observation proves the relevance and effectiveness of analytical study around SIM, more precisely, around the response regime with two impacts per cycle (i.e., resonance captures).

More specifically about experimental results, several points should be pointed out. Firstly , different basic periodic and transient response regimes are observed and analyzed from the experimental results under excitation with a fixed frequency. In addition, more complicated responses are observed but they can be explained by these basic response regimes. Then, they are applied to explain the complicated variation of response regimes, not only for excitation with a fixed frequency and a range frequency, but also for transient excitation. All observations

31

here prove the important role of the regime with two impacts per cycle. Under transient excitation, this role is further demonstrated by the separate activation of VI NES of different clearances. This separate activation of VI NES with two impacts per cycle can be applied to control vibration at different levels of displacement amplitude. Sometimes, although the addition of VI NES cannot improve the efficiency of vibration control, the impacts are scattered and their strengths are reduced.

In a word, many aspects of the dynamics are further explained by the analytical, numerical and experimental studies, but other factors, such as the friction between LO and VI NES, inclinations of clearances and impact models, should be considered in the analytical treatment to improve the accuracy of explanation.

Acknowledgments

[1] D. M. McFarland, L. A. Bergman, A. F. Vakakis, Experimental study of nonlinear energy pumping occurring at a single fast frequency, Int. J. Non-Linear Mech. 40 (6) (2005) 891–899.

[2] E. Gourc, G. Michon, S. Seguy, A. Berlioz, Experimental investigation and design optimization of targeted energy transfer under periodic forcing, J. Vib. Acoust. 136 (2) (2014) 021–021.

[3] R. Bellet, B. Cochelin, P. Herzog, P.-O. Mattei, Experimental study of targeted energy transfer from an acoustic system to a nonlinear membrane absorber, J. Sound Vib. 329 (14) (2010) 2768–2791.

[4] P.-O. Mattei, R. Ponçot, M. Pachebat, R. Côte, Nonlinear targeted energy transfer of two coupled cantilever beams coupled to a bistable light attachment, J. Sound Vib. 373 (2016) 29–51.

[5] S. Benacchio, A. Malher, J. Boisson, C. Touzé, Design of a magnetic vibration absorber with tunable stiffnesses, Nonlinear Dyn. (2016) 1–19.

[6] C.-H. Lamarque, O. V. Gendelman, A. T. Savadkoohi, E. Etcheverria, Targeted energy transfer in mechanical systems by means of non-smooth nonlinear energy sink, Acta Mech. 221 (1-2) (2011) 175–200.

[7] P. Lieber, D. Jensen, An acceleration damper: development, design and some applications, Trans. ASME 67 (10) (1945) 523–530.

[8] R. A. Ibrahim, Vibro-impact dynamics: modeling, mapping and applications, Vol. 43, Springer Science & Business Media, 2009.

[9] V. I. Babitsky, Theory of vibro-impact systems and applications, Springer Science & Business Media, 2013.

[10] S. Masri, T. Caughey, On the stability of the impact damper, J. Appl. Mech. 33 (3) (1966) 586–592.

[11] C. Bapat, N. Popplewell, K. McLachlan, Stable periodic motions of an impact-pair, J.Sound Vib. 87 (1) (1983) 19–40.

[12] N. Popplewell, C. Bapat, K. McLachlan, Stable periodic vibroimpacts of an oscillator, J. Sound Vib. 87 (1) (1983) 41–59.

[13] C. Bapat, S. Sankar, Single unit impact damper in free and forced vibration, J. Sound Vib. 99 (1) (1985) 85–94.

33

[14] F. Peterka, More detail view on the dynamics of the impact damper, Mechanics, Automatic Control and Robotics 3 (14) (2003) 907–920.

[15] S. Masri, Effectiveness of two-particle impact dampers, J. Acoust. Soc. Am 41 (6) (1967) 1553–1554.

[16] S. Masri, Analytical and experimental studies of multiple-unit impact dampers, J. Acoust. Soc. Am 45 (5) (1969) 1111–1117.

[17] C. Cempel, The multi-unit impact damper: equivalent continuous force approach, J. Sound Vib. 34 (2) (1974) 199–209.

[18] C. Bapat, S. Sankar, N. Popplewell, Experimental investigation of controlling vibrations using multi-unit impact damper, Shock Vib Bull 4 (1983) 1–12.

[19] N. Popplewell, Y. Muzyka, C. Bapat, K. McLachlan, Stable periodic motion of multiple-unit impacting mechanisms, J. Sound Vib. 86 (4) (1983) 587–593.

[20] C. Bapat, S. Sankar, Multiunit impact damper- re-examined, J. Sound Vib. 103 (4) (1985) 457–469.

[21] Y. Lee, A. F. Vakakis, L. Bergman, D. McFarland, G. Kerschen, F. Nucera, S. Tsakirtzis, P. Panagopoulos, Passive non-linear targeted energy transfer and its applications to vibration absorption: a review, P. I. Mech Eng. K-J Mul. 222 (2) (2008) 77–134.

[22] A. F. Vakakis, O. Gendelman, L. Bergman, D. McFarland, G. Kerschen,

Y. Lee, Nonlinear targeted energy transfer in mechanical and structural sys-
tems, Vol. 156, Springer Science & Business Media, 2008.

[23] F. Nucera, A. Vakakis, D. McFarland, L. Bergman, G. Kerschen, Targeted
energy transfers in vibro-impact oscillators for seismic mitigation, Nonlinear
Dyn. 50 (3) (2007) 651–677.

[24] F. Nucera, F. Lo Iacono, D. McFarland, L. Bergman, A. Vakakis, Application
of broadband nonlinear targeted energy transfers for seismic mitigation of a
shear frame: Experimental results, J. Sound Vib. 313 (1) (2008) 57–76.

[25] I. Karayannis, A. Vakakis, F. Georgiades, Vibro-impact attachments as shock
absorbers, P. I. Mech. Eng. C-J Mec. 222 (10) (2008) 1899–1908.

[26] Y. Lee, F. Nucera, A. Vakakis, D. McFarland, L. Bergman, Periodic orbits,
damped transitions and targeted energy transfers in oscillators with vibro-
impact attachments, Physica D 238 (18) (2009) 1868–1896.

[27] O. V. Gendelman, Bifurcations of nonlinear normal modes of linear oscilla-
tor with strongly nonlinear damped attachment, Nonlinear Dynamics 37 (2)
(2004) 115–128.

[28] O. Gendelman, Y. Starosvetsky, M. Feldman, Attractors of harmonically
forced linear oscillator with attached nonlinear energy sink i: Description
of response regimes, Nonlinear Dynamics 51 (1-2) (2008) 31–46.

[29] O. Gendelman, Analytic treatment of a system with a vibro-impact nonlinear
energy sink, J. Sound Vib. 331 (21) (2012) 4599–4608.

[30] E. Gourc, G. Michon, S. Seguy, A. Berlioz, Targeted energy transfer under harmonic forcing with a vibro-impact nonlinear energy sink: Analytical and experimental developments, J. Vib. Acoust. 137 (3) (2015) 031008.

[31] O. Gendelman, A. Alloni, Dynamics of forced system with vibro-impact energy sink, J. Sound Vib. 358 (2015) 301–314.

[32] G. Pennisi, C. Stéphan, G. Michon, Vibro-impact nes: A correlation between experimental investigation and analytical description, in: Sensors and Instrumentation, Volume 5, Springer, 2016, pp. 137–142.

[33] T. Li, S. Seguy, A. Berlioz, Dynamics of cubic and vibro-impact nonlinear energy sink: Analytical, numerical, and experimental analysis, J. Vib. Acoust. 138 (3) (2016) 031–010.

[34] O. Gendelman, A. Alloni, Forced system with vibro-impact energy sink: Chaotic strongly modulated responses, Procedia IUTAM 19 (2016) 53–64.

[35] T. Li, S. Seguy, A. Berlioz, On the dynamics around targeted energy transfer for vibro-impact nonlinear energy sink, Nonlinear Dynamics (2016) 1–14doi:10.1007/s11071-016-3127-0.
URL http://dx.doi.org/10.1007/s11071-016-3127-0

[36] T. Li, S. Seguy, A. Berlioz, Optimization mechanism of targeted energy transfer with vibro-impact energy sink under periodic and transient excitation, Nonlinear Dynamics (2016) 1–19doi:10.1007/s11071-016-3200-8.
URL http://dx.doi.org/10.1007/s11071-016-3200-8

[37] E. Gourc, S. Seguy, G. Michon, A. Berlioz, B. Mann, Quenching chatter

36

565   instability in turning process with a vibro-impact nonlinear energy sink, J.
566   Sound Vib. 355 (2015) 392–406.

567 [38] B. Bergeot, S. Bellizzi, B. Cochelin, Analysis of steady-state response
568   regimes of a helicopter ground resonance model including a non-linear en-
569   ergy sink attachment, Int. J. Non-Linear Mech. 78 (2016) 72–89.

570 [39] F. Georgiades, A. F. Vakakis, G. Kerschen, Broadband passive targeted en-
571   ergy pumping from a linear dispersive rod to a lightweight essentially non-
572   linear end attachment, Int. J. Non-Linear Mech. 42 (5) (2007) 773–788.

573 [40] S. Tsakirtzis, G. Kerschen, P. N. Panagopoulos, A. F. Vakakis, Multi-
574   frequency nonlinear energy transfer from linear oscillators to mdof essen-
575   tially nonlinear attachments, Journal of Sound and Vibration 285 (1) (2005)
576   483–490.

577 [41] S. Tsakirtzis, P. N. Panagopoulos, G. Kerschen, O. Gendelman, A. F.
578   Vakakis, L. A. Bergman, Complex dynamics and targeted energy transfer
579   in linear oscillators coupled to multi-degree-of-freedom essentially nonlin-
580   ear attachments, Nonlinear Dynamics 48 (3) (2007) 285–318.

581 [42] B. Vaurigaud, A. T. Savadkoohi, C.-H. Lamarque, Targeted energy transfer
582   with parallel nonlinear energy sinks. part i: design theory and numerical
583   results, Nonlinear Dyn. 66 (4) (2011) 763–780.

584 [43] A. T. Savadkoohi, B. Vaurigaud, C.-H. Lamarque, S. Pernot, Targeted energy
585   transfer with parallel nonlinear energy sinks, part ii: theory and experiments,
586   Nonlinear Dyn. 67 (1) (2012) 37–46.

587 [44] Z. Lu, X. Lu, S. F. Masri, Studies of the performance of particle dampers

588   under dynamic loads, J. Sound Vib. 329 (26) (2010) 5415–5433.